Updatable Balanced Index for Fast On-device Search with Auto-selection Model

Yushuai Ji*, Sheng Wang*§, Zhiyu Chen[†], Yuan Sun[‡], and Zhiyong Peng*

*School of Computer Science, Wuhan University

[†] Amazon.com, Inc.

[‡] La Trobe Business School, La Trobe University

[yushuai, swangcs, peng]@whu.edu.cn, zhiyuche@amazon.com, yuan.sun@latrobe.edu.au

Abstract—Diverse types of edge data, such as 2D geo-locations and 3D point clouds, are collected by sensors like lidar and GPS receivers on edge devices. On-device searches, such as k-nearest neighbor (kNN) search and radius search, are commonly used to enable fast analytics and learning technologies, such as kmeans dataset simplification using kNN. To maintain high search efficiency, a representative approach is to utilize a balanced multi-way KD-tree (BMKD-tree). However, the index has shown limited gains, mainly due to substantial construction overhead, inflexibility to real-time insertion, and inconsistent query performance. In this paper, we propose UnIS to address the above limitations. We first accelerate the construction process of the BMKD-tree by utilizing the dataset distribution to predict the splitting hyperplanes. To make the continuously generated data searchable, we propose a selective sub-tree rebuilding scheme to accelerate rebalancing during insertion by reducing the number of data points involved. We then propose an auto-selection model to improve query performance by automatically selecting the optimal search strategy among multiple strategies for an arbitrary query task. Experimental results show that UnIS achieves average speedups of 17.96× in index construction, 1.60× in insertion, 7.15× in kNN search, and 1.09× in radius search compared to the BMKD-tree. We further verify its effectiveness in accelerating dataset simplification on edge devices, achieving a speedup of 217× over Lloyd's algorithm.

I. INTRODUCTION

Edge devices such as autonomous vehicles [41] and drones [46] are typically equipped with sensors like GPS and lidar. These sensors continuously generate large volumes of data points [19], such as 2D geo-location from GPS and 3D point clouds [13] from lidar. The on-device search, such as *k*NN search and radius search, can be applied to such data for efficient analysis and learning [14], [29], [47], [48], [54]. For example, *k*NN search is the core idea behind several clustering accelerators [21], [22], which can improve k-means efficiency in classification [25] and segmentation [20], [34].

The most popular method to support on-device search is through the use of indices. Specifically, an index is a data structure that improves search efficiency at the expense of additional storage space. In general, the indexes that are widely used can be classified into three categories [32]: 1) table-based indexes, 2) graph-based indexes, and 3) tree-based indexes. However, table-based and graph-based indexes cannot improve on-device search efficiency, as both inherently trade

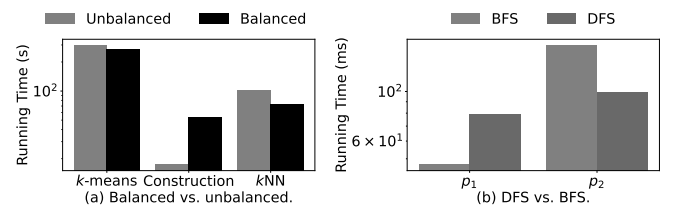


Fig. 1. Performance comparisons of the balanced multi-way KD-tree.

off result completeness for efficiency, and ensuring exactness requires traversing all data points. Tree-based indexes can avoid unnecessary computations when searching for exact results by assigning similar data points to the same sub-space. For example, given a query point \mathbf{p}^* , kNN will traverse the tree iteratively from the root node and apply the *triangle inequality* [16] to prune the sub-spaces that are far from \mathbf{p}^* . Once the traversal on the unpruned sub-spaces is done, the exact results will be returned.

However, when dealing with large-scale datasets, tree-based indexes often struggle to efficiently retrieve up-to-date data for supporting real-time downstream analytics and learning [21], [39], [55]. For example, indexes such as balanced multi-way KD-trees (BMKD-trees) [33] can accelerate the updatable k-means process [21] by improving the efficiency of kNN search. Yet in practice, when processing large-scale datasets—for instance, clustering 5 million data points from the ArgoPC [3]—these accelerators, such as Dask-means [21], achieve only a $1.07\times$ average speedup over the traditional k-means [28]. The reduced acceleration is due to the substantial indexing overhead, limited support for real-time insertion, and inconsistent query performance. Details are provided below.

Time-Intensive Construction Process. Constructing a BMKD-tree can reduce the average search path length, which is critical for improving query performance. However, this process requires sorting to compute splitting hyperplanes that divide the dataset into equally sized subspaces, which is time-consuming [53]. As shown in Fig. 1(a), the BMKD-tree outperforms the unbalanced one in kNN. Nonetheless, its construction takes more than four times longer. Hence, although kNN search using BMKD-trees can accelerate the k-means algorithm more effectively, the time saved in searching is offset by the high index construction cost.

Rebuilding Overhead. Updating-intensive operations disrupt

[§]Sheng Wang is the corresponding author.

the structure of BMKD-trees, hindering efficient access to the latest data points [49]. The tree periodically rebuilds to ensure that queries efficiently retrieve the most recent data points, but the rebuilding process is time-consuming. A classical method to improve rebuild efficiency by using the *scapegoat strategy* [12], which involves the parallel rebuilding of sub-trees to achieve balance. However, when facing a large volume of real-time insertions, sub-tree rebuilding occurs more frequently, making the strategy less effective.

Inconsistent Query Performance. No single search strategy can perform well for all queries. For example, in Fig. 1(b), we perform kNN queries with two points, \mathbf{p}_1 and \mathbf{p}_2 . We use two traversal strategies to explore the search space: Breadth-First Search (BFS) and Depth-First Search (DFS). The DFS-based strategy is more efficient for \mathbf{p}_1 , while the BFS-based strategy is better for \mathbf{p}_2 . This is because the dimensionality and distribution of the dataset have varying effects on the DFS and BFS search efficiency [37]. Manual selection of optimal strategies is impractical due to lacking a simple and discernible rule [45]. A feasible solution to improve selecting optimal strategies' efficiency is using auto-selection models [36]. However, existing auto-selection methods [7], [42] encounter inefficiencies during training sample generation, attributed to the lack of a fast and informative feature extraction method.

To address these challenges, we propose UnIS, an updatable balanced index for fast on-device search with an auto-selection model. It is designed to accelerate both search and update operations for edge data over the BMKD-tree. Overall, we make the following contributions in this paper:

- To accelerate the construction of the BMKD-tree, we leverage data distribution to predict splitting hyperplanes instead of performing sorting, thereby improving the efficiency of space partitioning (see Section IV).
- We propose a selective sub-tree rebuilding scheme that identifies and reconstructs unbalanced sub-tree portions, thereby accelerating index rebalancing and improving updating efficiency (see Section V).
- To achieve fast exact searches for arbitrary query tasks, we design a lightweight auto-selection model to predict the optimal search strategy from a set of candidate strategies for each query task over the BMKD-tree (see Section VI).
- Experiments show that UnIS achieves average speedups of 17.96× in index construction, 1.60× in insertion, 7.51× in kNN search, and 1.09× in radius search. We also verify its effectiveness in accelerating k-means on edge devices, achieving an average speedup of 217× (see Section VII).

II. RELATED WORK

KD-tree and Its Variants. The traditional method of constructing a KD-tree [8] is to recursively generate a splitting hyperplane by averaging the maximum and minimum values in a specific dimension to split the space into two. However, using the average does not partition the dataset evenly, potentially leading to high vector volume in certain sub-spaces. Hence, the sub-spaces require more partitions compared to those with

fewer vectors, resulting in increased tree depth (longer average search path length [9]) and impairing query performance.

Instead of using means, Friedman et al. [16] propose using medians to construct a balanced KD-tree to partition the dataset into sub-spaces evenly, ensuring that leaf nodes reside at the same tree depth level. However, the traditional median-finding scheme involves sorting [16], [53], which is known for its time-intensive nature. To address the limitation, Brown [53] pre-sorts the data in each dimension and hence decreases the sorting time in construction. Blelloch et al. [10] reduce the sorting time by applying the well-known *Z-order* technique, which reduces vectors' dimensionality, to improve construction efficiency. However, as dimensionality increases, the sorting time grows significantly, leading to higher time costs, rendering both methods ineffective in accelerating index construction beyond four dimensions.

To further improve the query performance, Procopiuc et al. [9], [33] utilize the idea of the median-finding scheme within the multi-way KD-tree, which splits space into more than two sub-spaces to reduce the search path length on average. The index determines an appropriate partition number through experimentation [9], testing different values of partition number to find the one that achieves the optimal query performance. However, sorting is still conducted to locate the equidistant points for space partitioning after determining the partition number. Yesantharao et al. [50] partition the dataset into subsets and construct a balanced multi-way KD-tree for each subset, thereby reducing the sorting time as each subset is sorted individually, yet sorting is still required.

Recently, several studies [18], [24] have utilized learning techniques [23] on tree-structured indexes, which use machine learning (ML) models to capture the relationship of the position of vectors through the Cumulative Distribution Function (CDF) of the dataset. However, training ML models [7], [11] to meet exact search requirements takes a substantial amount of time before they positively impact query performance.

Index Insertion and Rebalance. To ensure efficient retrieval of continuously generated vectors, existing indexes periodically rebalance themselves during vector insertion [49], utilizing either out-of-place or in-place insertion technologies. Out-of-place insertion [40], [44] periodically merges delta indexes (rebuilt by the inserted vectors) into the base index via a global rebuilding process. However, the process requires additional memory to construct a duplicate index, which replaces the unbalanced one once the index is fully constructed.

In contrast, in-place insertion [49] involves inserting vectors into the existing index with dynamic rebalancing. Current indexes using in-place insertion include tree-structured indices [12], [49] and cluster-based indices [26], [44]. Notably, cluster-based indices replace the node of the tree-structured index with clusters and thus can be regarded as a type of tree-structured index. Tree-structured index rebuilding typically employs the scapegoat strategy [12], [17], [50] to accelerate the rebalancing process by reconstructing sub-trees rather than fully rebuilding the entire tree. When facing update-intensive tasks, the tree-

TABLE I SUMMARY OF NOTATIONS.

Notation	Description
$n \in \mathbb{Z}^+$	The dataset size.
$k \in \mathbb{Z}^+$	The k nearest neighbors.
$k \in \mathbb{Z}^+$	The k clusters.
$\mathbf{p} = (x_1, x_2,, x_d) \in \mathbb{R}^d$	The vector.
$\mathbf{D} = \{\mathbf{p}_i\}_{i=1}^n \in \mathbb{R}^{n \times d}$	The dataset.
T^{1}	The tree-structured index.
$c \in \mathbb{Z}^+$	The leaf node capacity.
$\delta \in (0,1)$	The sampling rate.
$d \in \mathbb{Z}^+$	The vector data dimension.
$\mathbf{P}\subseteq\mathbf{D}$	The vector subset.
$\mathbf{O},\mathbf{o}\in\mathbb{R}^d$	The pivot set and the pivot.
${f M}$	The recursive CDF model.

structured indexes undergo frequent partial rebuilds, resulting in the strategy being unable to reduce the number of vectors involved in rebuilding compared to global rebuilding.

Optimal Search Strategy Selection. The lack of a discernible rule makes it challenging to determine the optimal search strategy for an arbitrary query [45]. An effective method to address this limitation is the auto-selection model [15], which trains the classifier using meta-knowledge (or meta-features) extracted from previous similar tasks to identify the top-performing methods for unseen tasks.

Most auto-selection models [7], [36], [42] aim to find the fastest or most accurate method for a given task. For example, Unik [42] models the fastest k-means algorithm selection as a multi-label classification problem. It extracts features and trains a classifier from samples to predict the optimal algorithm pipeline for accelerating k-means clustering tasks. However, Unik only extracts basic features for each task, such as the data volume for the dataset, which cannot gain a high prediction accuracy for arbitrary datasets. TRIO [15] extracts more features to improve prediction accuracy, yet it overlooks the time costs, for instance, those incurred by utilizing the graph convolutional neural network [27] for feature extraction.

Remarks. We can observe that: 1) the balanced KD-tree and its variants, such as BMKD-tree, can provide fast queries, but they still consume too much time on construction; 2) all insertion methods discussed necessitate significant time for index reconstruction to keep balance, thereby ensuring efficient queries; 3) existing auto-selection models suffer from inefficiencies in feature extraction due to the absence of a fast and informative feature extraction method.

III. PRELIMINARIES

A. Notations

We use different text formatting styles to represent mathematical concepts: plain letters for scalars, bold letters for vectors, capitalized letters for objects, and bold capitalized letters for a set containing data points. For example, x stands for a scalar, \mathbf{p} represents a data point, N denotes a node, and \mathbf{D} represents a dataset. Without loss of generality, we denote the d-dimensional Euclidean space as \mathbb{R}^d , the set of positive real numbers as \mathbb{R}^+ , and the set of positive integers as \mathbb{Z}^+ .

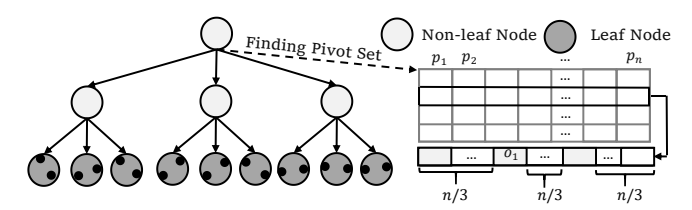


Fig. 2. A balanced multi-way KD-tree with a partition number of t = 3.

We represent the set of scalar values from the j_1 -th to j_2 -th elements in the i-th dimension of \mathbf{D} as $\{x_{ij}\}_{i=j_1}^{j_2}$. The vector length is denoted by $|\cdot|$, and $\mathrm{dist}(\cdot)$ stands for the Euclidean distance measure. The notation details are presented in Table I.

B. Balanced Multi-way KD-tree

The balanced multi-way KD-tree [33], [50] consists of pivot sets, non-leaf nodes, and leaf nodes, as outlined below:

Definition 1. (*Pivot Set*) Given a dataset $\mathbf{D} = \{\mathbf{p}_i\}_{i=1}^n \in \mathbb{R}^{n \times d}$, the partition number denoted as t, and a specified dimension symbolized by j, a pivot set consists of ranked values denoted by $\mathbf{O} = \{\mathbf{o}_i\}_{i=1}^{t-1} \in \mathbb{R}^{t-1}$, where o_i corresponds to the value associated with the $\frac{i}{t}$ -th percentile of $\{x_{ij}\}_{i=0}^n$.

Definition 2. (Non-leaf Node) A non-leaf node is defined as $N = (\mathbf{O}, \mathbf{C}_{nl}, j)$, where \mathbf{O} represents the pivot set, \mathbf{C}_{nl} is the children of N, and j stands for the specific dimension. Here, $\mathbf{C}_{nl}[i]$ denotes the i-th sub-tree rooted at N.

Definition 3. (*Leaf Node*) A leaf node is denoted as $N_l = (\mathbf{C}_l, c)$, where \mathbf{C}_l represents the data point set, and c is the leaf node capacity.

An example of balanced multi-way KD-tree construction is shown in Fig. 2. The construction commences by partitioning the space by selecting two pivots, denoted as o_1 and o_2 , along the specific dimension. One-third of the points lie below o_1 along that dimension, while two-thirds lie below o_2 , ensuring that the dataset is evenly distributed into three sub-spaces. We then recursively select each dimension and repeat the partitioning process until the number of points in each node falls below the leaf node capacity c=2.

Definition 4. (k Nearest Neighbors (kNN) Search) Given a dataset $\mathbf{D} = \{\mathbf{p}_i\}_{i=1}^n \in \mathbb{R}^{n \times d}$, a query point $\mathbf{p}^* \in \mathbb{R}^d$, and an integer $k \in \mathbb{Z}^+$, kNN returns k data points in \mathbf{D} that are the most similar to \mathbf{p}^* , i.e., it retrieves $\mathbf{P} \subseteq \mathbf{D}$ with k points such that: $\forall \mathbf{p} \in \mathbf{P}$ and $\forall \mathbf{p}' \in \mathbf{D} - \mathbf{P}$, we have $dist(\mathbf{p}^*, \mathbf{p}) < dist(\mathbf{p}^*, \mathbf{p}')$.

Definition 5. (*Radius Search (RS*)) Given a dataset $\mathbf{D} = \{\mathbf{p}_i\}_{i=1}^n \in \mathbb{R}^{n \times d}$, a query point $\mathbf{p}^* \in \mathbb{R}^d$, and a search radius $r \in \mathbb{R}$, the radius search retrieves all points $\mathbf{p} \in \mathbb{R}^d$ that satisfy the condition $dist(\mathbf{p}, \mathbf{p}^*) \leq r$.

C. Common Pruning Technologies

We introduce the concepts of *Minimum Bounding Rectangle* and *Minimum Bounding Ball*, along with pruning strategies aimed at avoiding unnecessary computations in queries.

Definition 6. (Minimum Bounding Rectangle (MBR)) Given a dataset $\mathbf{D} = \{\mathbf{p}_i\}_{i=1}^n \in \mathbb{R}^{n \times d}$, a subset $\mathbf{P} \subseteq \mathbf{D}$, the minimum bounding rectangle, denoted by $R = (\mathbf{bp}, \mathbf{tp})$, is the smallest d-dimensional bounding rectangle encompassing all points in \mathbf{P} , where $\mathbf{tp} = (tp_1, tp_2, \cdots, tp_d) \in \mathbb{R}^d$ is the upper bound, while $\mathbf{bp} = (bp_1, bp_2, \cdots, bp_d) \in \mathbb{R}^d$ is the lower bound.

Definition 7. (Minimum Bounding Ball (MBB)) Given a dataset $\mathbf{D} = \{\mathbf{p}_i\}_{i=1}^n \in \mathbb{R}^{n \times d}$, a subset $\mathbf{P} \subseteq \mathbf{D}$, the MBB, denoted as $B = (\mathbf{o}, r)$, is the smallest d dimensional bounding ball containing all the points in \mathbf{P} , with its center located at the centroid $\mathbf{o} \in \mathbb{R}^d$. The radius of MBB is calculated by $r = \max_{\mathbf{p} \in \mathbf{P}} dist(\mathbf{p}, \mathbf{o})$.

Lemma 1. (Rectangle-Rectangle Pruning) Given a dataset $\mathbf{D} = \{\mathbf{p}_i\}_{i=1}^n \in \mathbb{R}^{n \times d}, \ a \ subset \ \mathbf{P} \subseteq \mathbf{D}, \ which \ is compressed \ by \ the \ MBR, \ R_1 = (\mathbf{bp}, \mathbf{tp}), \ where \ \mathbf{tp} = (tp_1, tp_2, \cdots, tp_d) \in \mathbb{R}^d \ and \ \mathbf{bp} = (bp_1, bp_2, \cdots, bp_d) \in \mathbb{R}^d, \ and \ a \ query \ range \ R_2 = (\mathbf{bp}^1, \mathbf{tp}^1), \ where \ \mathbf{bp}^1 = (bp_1^1, bp_2^1, \cdots, bp_d^1) \in \mathbb{R}^d \ and \ \mathbf{tp}^1 = (up_1^1, up_2^1, \cdots, up_d^1) \in \mathbb{R}^d, \ if \ the \ following \ equation \ holds:$

$$\max(bp_i, bp_i^1) \le \min(tp_i, tp_i^1), \forall i = 1, \cdots, d, \tag{1}$$

then the two MBRs intersect.

Since R_1 intersects with R_2 , pruning R_2 is not feasible.

Lemma 2. (Ball-Ball Pruning) Given a dataset $\mathbf{D} = \{\mathbf{p}_i\}_{i=1}^n \in \mathbb{R}^{n \times d}$, a subset $\mathbf{P} \subseteq \mathbf{D}$, which is compressed by the MBB, $B = (\mathbf{o}, r_o)$ with a center located at the data point $\mathbf{o} \in \mathbb{R}^d$ and the radius $r_o \in \mathbb{R}^+$, a query point $\mathbf{p}^* \in \mathbb{R}^d$, and a search radius $r \in \mathbb{R}^+$, if $dist(\mathbf{o}, \mathbf{p}^*) > r_o + r$, the points in \mathbf{P} can be pruned.

Lemma 3. (Rectangle-Ball Pruning) Given a dataset $\mathbf{D} = \{\mathbf{p}_i\}_{i=1}^n \in \mathbb{R}^{n \times d}$, a subset $\mathbf{P} \subseteq \mathbf{D}$ compressed by the MBR, $R = (\mathbf{bp}, \mathbf{tp})$, where $\mathbf{tp} = (tp_1, tp_2, \cdots, tp_d) \in \mathbb{R}^d$ and $\mathbf{bp} = (bp_1, bp_2, \cdots, bp_d) \in \mathbb{R}^d$, and a query point $\mathbf{p}^* = (x_1, x_2, \cdots, x_d) \in \mathbb{R}^d$ with a search radius r, the minimum distance between \mathbf{p}^* and the MBR, represented by $dist_{min}(\mathbf{p}^*, R)$, is calculated as following:

$$dist_{min}(\mathbf{p}^*, R) = \sqrt{\sum_{i=1}^{d} (x_i - x')^2}, \ x' = \begin{cases} bp_i, & x_i < bp_i; \\ tp_i, & x_i > tp_i; \\ x_i, & otherwise. \end{cases}$$

Then **P** is pruned if $dist_{min}(\mathbf{p}^*, R)$ is greater than r.

IV. FAST CONSTRUCTION OF BALANCED INDEX

Before delving into the balanced multi-way KD-tree construction process, we accelerate the space partition procedure by introducing two key steps: 1) instead of experimenting to test which t yields the highest query efficiency, we optimize the number of comparisons on average in queries to find an appropriate partition number in Section IV-A, and 2) we design a lightweight ML model to approximate the CDF of the dataset for pivot set prediction to avoid sorting in Section IV-B. Subsequently, we elaborate on the implementation of the method in the construction process in Section IV-C.

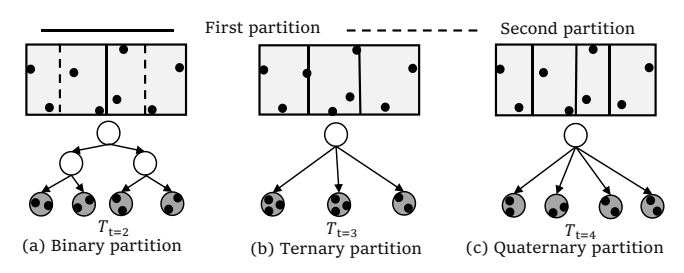


Fig. 3. Impact of t values on AEPL with leaf node capacity c=3. Notably, in (a), since the data points in each subtree after the first partition do not fall below c, a second partitioning is required, represented by the dashed lines.

A. Determining Partition Number

We first introduce a key metric, the average external path length (AEPL) [9], [30], to evaluate the average query performance of the balanced multi-way KD-tree. Then we analyze the impact of t on the AEPL of the index. Based on the analysis, we formulate the choice of t for a given dataset as an optimization problem and approximate the solution.

Definition 8. (Average External Path Length (AEPL)) Given a dataset $\mathbf{D} = \{\mathbf{p}_i\}_{i=1}^n \in \mathbb{R}^{n \times d}$, the AEPL of a tree-structured index built on \mathbf{D} , denoted as H, is defined as:

$$H = \frac{\sum_{i=1}^{n} e(\mathbf{p}_i)}{n},\tag{3}$$

where $e(\mathbf{p}_i)$ denotes the number of comparisons from the root node to the leaf node storing \mathbf{p}_i .

Based on Definition 8, for a balanced multi-way KD-tree T, if each leaf node contains the same number of data points c_0 , the AEPL of T, denoted as H_T , can be expressed as:

$$H_T = \left[c_0 \times \left(\frac{t^2}{2} + \frac{t}{2} - 1\right)\right]^{\lceil \log \frac{n}{c} \rceil}.$$
 (4)

However, due to the inability to evenly divide an odd number of data points, the distribution results in one leaf node containing one more point than the others, as exemplified by the split of 7 points into groups of 3 and 4. Therefore, the value of c_0 can be either $\lfloor \frac{n}{t(\lceil \log_t \frac{n}{c} \rceil)} \rfloor$ or $\lceil \frac{n}{t(\lceil \log_t \frac{n}{c} \rceil)} \rceil$.

To approximate H_T , we can determine c_0 using rounding technology: specifically, we define Δc_0 as follows:

$$\Delta c_0 = \frac{n}{t^{\lceil \log_t \frac{n}{c} \rceil}} - \lfloor \frac{n}{t^{\lceil \log_t \frac{n}{c} \rceil}} \rfloor. \tag{5}$$

Hence, we acquire c_0 by comparing Δc_0 with 0.5 using rounding, expressed as follows:

$$c_0 = \begin{cases} \left\lfloor \frac{n}{t^{\lceil \log_t \frac{n}{c} \rceil}} \right\rfloor, & \text{if } \Delta c_0 \le 0.5; \\ \left\lceil \frac{n}{t^{\lceil \log_t \frac{n}{c} \rceil}} \right\rceil, & \text{if } \Delta c_0 > 0.5; \end{cases}$$
(6)

Effect of t **on AEPL and Query Efficiency.** Adjusting t for a given dataset results in changes in the AEPL value during the construction process. For instance, utilizing t=2 as in the balanced KD-tree may not always be the optimal choice to achieve AEPL-optimality across various datasets. In Fig. 3, we implement binary, ternary, and quaternary partitions for index construction, considering 8 points. The AEPL values for each index are $H_{T_{t=2}}=2$, $H_{T_{t=3}}=1.25$, and $H_{T_{t=4}}=2.25$. Remarkably, $H_{T_{t=3}}$ is the lowest, indicating that t=3 achieves

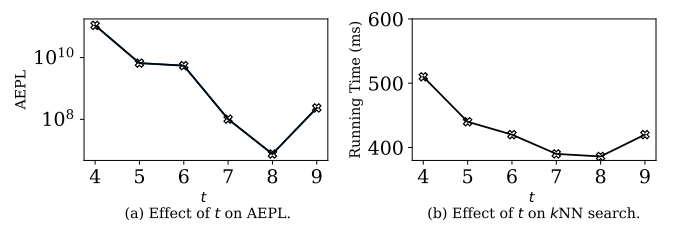


Fig. 4. Impact of different values of t on AEPL and kNN efficiency (100 tasks) with leaf capacity c=30 on ArgoPC.

AEPL-optimality for constructing the index. Moreover, Fig. 4 presents the AEPL and kNN search efficiency under different t values on 1 million data points from ArgoPC [3]. We observe that as t increases, both AEPL and query runtime (100 query tasks) first decrease and then increase, reaching their minimum at t=8. Hence, we use AEPL to measure query efficiency and define the AEPL-optimal criterion as follows:

Definition 9. (*AEPL-optimal Criterion*) Given a dataset $\mathbf{D} \in \mathbb{R}^{n \times d}$ and a leaf node capacity c, a balanced multi-way KD-tree is said to be AEPL-optimal when the following objective is minimized with respect to the partition number $t \in \mathbb{Z}^+$:

$$H_T = \min_{t \in \mathbb{Z}^+} \left[c_0 \times \left(\frac{t^2}{2} + \frac{t}{2} - 1 \right) \right]^{\lceil \log_t^{\frac{n}{c}} \rceil}. \tag{7}$$

A classical way to obtain the minimum of an objective function involves taking its derivative and setting the derivative equal to 0 to find critical points. However, the rounding symbol and $t \in \mathbb{Z}^+$ render H_T non-continuous, leading to a lack of differentiability. To address the limitation, we adopt the simulated annealing approach [35] to efficiently search for the optimal partition number t^* , where candidate values of t are iteratively evaluated and probabilistically accepted to balance exploration and convergence.

B. Accelerating Pivot Set Finding

Once t^{st} is determined, instead of relying on sorting, which needs to locate each pivot by determining the position of each data point in the dataset, our focus shifts to identifying the positions of pivots. Therefore, we design a lightweight ML model called two-stage regression model to avoid unnecessary computations by using a small sample to approximate the CDF of the dataset, then utilizing the CDF to filter out irrelevant points and predict the pivot set in the remaining points.

Two-stage Regression Model. To estimate the CDF of a dataset in a given dimension $\mathbf{x} = \{x_1, x_2, \cdots, x_{n_1}\}$ and fit arbitrary nonlinear forms, we propose a two-stage regression model. The model first clusters similar data and then applies separate linear models to each cluster, allowing local trends to be captured and improving the overall fitting performance.

The model consists of two stages: the first stage contains the root model, responsible for estimating the CDF value for each data point and clustering data points with similar CDF values into l clusters, and the second stage consists of l submodels, each trained on the clusters to precisely compute their respective CDFs. We generate samples to support the root

```
Algorithm 1: CDF_Training(\mathbf{x}'_{n_1})
```

```
Input: x: the training set.
   \mathbf{x}'_{n_1} \leftarrow \text{Generate sample over } \mathbf{x};
   \operatorname{Sort}(\mathbf{x}_{n_1}');
   \mathbf{T} \leftarrow [][];
                                                // 2-dimension array
   \mathbf{T}_0 \leftarrow [];
                                                // 1-dimension
   for i \leftarrow 0 up to |\mathbf{x'_{n_1}}| do
         T_0.add((\mathbf{x}'_{n_1}[i], i/|\mathbf{x}'_{n_1}|));
   \mathbf{M} \leftarrow [];
                                                // 1-dimension array
   The root model M[0] is trained on T[0][0];
   Partition T_0 into T by calling M[0];
   for i \leftarrow 0 up to l do
         Training the sub-model M[i+1] on T[i];
12 return M;
```

model, which approximates the CDF of the dataset and divides the dataset into l clusters based on CDF values, each assigned an ID. The mapping between x_i , where $i = 1, 2, \dots, n_1$, and the ID of clusters $U = \{u | u < l, u \in \mathbb{Z}^+\}$ is expressed as:

$$u = l\alpha x_i + l\beta,\tag{8}$$

where α represents the slope, β signifies the intercept, and our objective is to minimize the sum of squared residuals (SSR).

Two notable points are worth mentioning: 1) to ensure differentiability when utilizing derivative-based methods for finding the optimal solution, we treat u as a continuous value, and 2) due to $l \in \mathbb{Z}^+$, obtaining the optimal solution through partial derivatives is not feasible. Instead, we calculate the partial derivatives of the objective with respect to α and β , and test different values of l to find the optimal solution (see Section VII-B). Hence, we take derivatives for α and β and set each derivative to 0, the derived expressions for α and β with respect to l can be presented as follows:

$$\begin{pmatrix} \alpha \\ \beta \end{pmatrix} = \frac{1}{l} \begin{pmatrix} \sum_{i=1}^{n} x_i^2 & \sum_{i=1}^{n} x_i \\ \sum_{i=1}^{n} x_i & \sum_{i=1}^{n} 1 \end{pmatrix}^{-1} \begin{pmatrix} \sum_{i=1}^{n} x_i u_i \\ \sum_{i=1}^{n} u_i \end{pmatrix}. \tag{9}$$

We use symbols to simplify Equation (9), like $S_x = \sum_{i=1}^n x_i$, $S_{x^2} = \sum_{i=1}^n x_i^2$, $S_u = \sum_{i=1}^n u_i$, and $S_{xu} = \sum_{i=1}^n x_i u_i$. Hence, α and β can be expressed as follows:

$$\alpha = \frac{1}{l} \times \frac{n \times S_{xu} - S_x \times S_u}{n \times S_{x^2} - (S_x)^2}, \beta = \frac{1}{l} \times \frac{S_u - \alpha \times S_x}{n}.$$
 (10)

After segmenting the dataset via the root model, we train each sub-model on the corresponding cluster. Instead of minimizing SSR, employing *piecewise linear fitting* (PLF) [43] is a preferable choice. This is because, although both models can estimate the CDF effectively, minimizing SSR necessitates traversing all data points to obtain S_x , S_u , S_{x^2} , and S_{xu} . In contrast, employing PLF only requires obtaining the maximum and minimum values of the dataset to support model training, thereby reducing the time complexity.

CDF Model Training. Algorithm 1 outlines the process for training the CDF model, denoted as M. We use T_0 to represent the training set for the root model (line 4) and T to represent an array storing training clusters for the sub-models (line 4). All $(\mathbf{x}'[i], \frac{i}{|\mathbf{x}'|})$ pairs are inserted into T_0 , where $\frac{i}{|\mathbf{x}'|}$

Algorithm 2: Build_Index(\mathbf{D} , d')

Input: D: the dataset, d': the tree depth.

Output: N: the root node.

- 1 **Default Values:** $i \leftarrow 0, j \leftarrow (n-1), d' \leftarrow 0$, Root Node N.
- 2 $d' \leftarrow d' \mod d$;
- $\mathbf{X} \leftarrow \{x_{i_1d'}\}_{i_1=i}^{j};$
- 4 if $|\mathbf{D}| < c$ then
- 5 | Store the vectors in N and **return** N;
- $\mathbf{6}$ Find t by the distribution-aware partition method;
- 7 $\mathbf{F} \leftarrow \text{CDF_Training}(\mathbf{X});$
- 8 Predict the pivot set O by calling F;
- 9 Partition **D** into $\mathbf{D}_1, \mathbf{D}_2, \cdots, \mathbf{D}_{(t-1)}$ using **O** and d';
- 10 for $i \leftarrow 0$ up to (t-1) do
- 11 | $N.\text{child}[i] \leftarrow \text{Build_Index}(\mathbf{D}_i, d');$

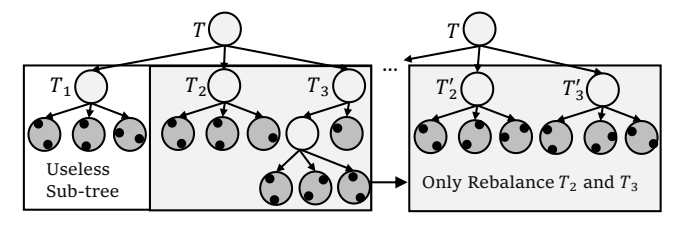


Fig. 5. An example of the rebalance process.

represents the CDF value for the training tuple, calculated as its index in the sorted dataset divided by the dataset size $(|\mathbf{x}'|)$ (line 6). Each training tuple is processed by the root model, which predicts a CDF value scaled by the number of sub-models. The training tuple is then divided into multiple training subsets, which are used to train the sub-models.

C. Time-efficient Construction Process

After introducing the above two key steps to accelerate space partitioning, we explore their implementation in the construction process. Algorithm 2 shows the construction process, and we first calculate t (see Section IV-A) and estimate the CDF model M by the two-stage regression model (line 7). Once M is obtained, we use it to exclude points that cannot be the pivot set O and find O among the remaining candidates.

Specifically, each pivot $o \in \mathbf{O}$ has a corresponding quantile q, such as the median's quantile being 0.5. To predict each pivot o, we utilize \mathbf{M} to scan the dataset, including the data in the pivot candidate set when the quantile falls within the range $[q-\kappa,q+\kappa]$, where κ represents a predefined error bound and lies within the range $[0,\frac{1}{t}]$. Taking the prediction of the median as an example, κ lies within the range [0,0.5]. If $\kappa=0$, then the interval [0.5,0.5] solely contains the value corresponding to 0.5, potentially leading to an empty pivot candidate set. However, if $\kappa=0.5$, the prediction range expands to [0,1], including all data points as pivot candidates. Section VII-B suggests that 0.15 is a suitable choice.

Further, for each pivot o, we collect pivot candidates falling into $[q - \kappa, q + \kappa]$, sort them, and identify the median as o. Finally, \mathbf{D} undergoes partitioning into subsets based on the predicted pivots (line 9), and we continue this process recursively until \mathbf{D} reaches the leaf node capacity c (line 5).

Time Complexity Analysis. The time complexity equals the product of the time complexity of partition in each level and

tree depth h (h << n). At each level, the dataset is divided into t subsets, with each subset having n_i data points, and $\sum_{i=1}^t n_i = n$. For each subset, the time complexity comprises three parts: 1) the training process involves sampling and sorting, costing $O(\delta n_i + \delta n_i \log(\delta n_i))$, where δ is the sampling rate; 2) using the two-stage regression model to train M costs $O(5\delta n_i)$; 3) predicting the pivot set and partitioning the subset cost $O(2\delta n_i)$. Hence, the time complexity for each subset is $O(8h\delta n_i + h\delta n_i \log(h\delta n_i))$, where $\mathbf{n} = (n_1, n_2, \ldots, n_t)$ and $\sum_{i=1}^t n_i = n$. To derive the time complexity, we maximize this expression with respect to \mathbf{n} , as shown below:

$$\sum_{i=1}^{t} (8h\delta n_i + h\delta n_i \log(h\delta n_i)) \le 8h\delta n + h\delta n \log(h\delta n), \quad (11)$$

where h << n and thus we can regard h as a constant. Considering the highest order term in time complexity analysis, the time complexity is $O(h\delta n \log(h\delta n))$.

V. REAL-TIME IN-PLACE INSERTION

Before discussing the in-place insertion, we propose the selective sub-tree rebuilding scheme to improve its efficiency by expediting the rebalancing process. The scheme improves rebalance efficiency by excluding unnecessary parts of the unbalanced sub-tree rather than opting for an entire rebuild.

A. Selective Sub-tree Rebuilding Scheme

We find that the scapegoat strategy [12] may have unnecessary computations during the full rebuilding of unbalanced sub-trees, resulting in additional time costs. For example, in Fig. 5, the sub-tree T is identified as unbalanced, necessitating reconstruction involving 18 data points. However, to rebalance T, it is only necessary to reconstruct T_2 and T_3 , involving 12 data points. To accelerate the rebalancing process, we propose a selective sub-tree rebuilding scheme to filter out the irrelevant data points in reconstructions. To be specific, we first explore how to determine whether the tree is unbalanced based on the ω -balanced criterion [12]. Next, we identify which parts of the unbalanced sub-trees do not need reconstruction by dynamically maintaining two variables.

Definition 10. (ω -balanced Criterion) Considering a sub-tree rooted at node N within the incremental index, the sub-tree is ω -balanced if and only if it meets the following condition:

$$S(T(N.\mathbf{C}_{nl}[i])) < \frac{1}{(t-1)} \times \omega \times S(N), \tag{12}$$

where $i = 1, 2, \dots, t$, $\omega \in (0.5, 1)$ and S(N) is the number of data points in the sub-tree rooted at N.

We can extend Definition 10 to a set of sub-trees. Specifically, a set of sub-trees rooted at N, denoted as $T(\{N.\mathbf{C}_{nl}[j]\}_{j=i_0}^{j=i_1})$, where $0 < i_0 < i_1 < t$, represents the sub-trees from i_0 -th to i_1 -th of N. If it satisfies the following inequality, $T(\{N.\mathbf{C}_{nl}[j]\}_{j=i_0}^{i_1})$ is ω -balanced:

$$\mathcal{S}(T(N.\mathbf{C}_{nl}[j])_{j=i_0}^{j=i_1})) < \frac{i_1 - i_0}{(t-1)} \times \omega \times \mathcal{S}(N).$$
 (13)

If $T(N.\mathbf{C}_{nl}[i])$, where 0 < i < t, is unbalanced, we do not need to rebalance T(N); Otherwise, we define the sub-trees needing reconstruction as T_{reb} and add $T(N.\mathbf{C}_{nl}[i])$. We then recursively incorporate neighboring sub-trees of $T(N.\mathbf{C}_{nl}[i])$ until Inequality (13) is satisfied, and finally, reconstruct T_{reb} .

Pruning Unnecessary Rebalance Parts. The sub-tree $T(N.\mathbf{C}_{nl}[i])$ is unbalanced. We dynamically maintain two variables on minimize the number of data points in the sub-tree for rebuilding. The two variables are denoted as ζ , representing the number of data points in the sub-trees, and ψ , defined as a tuple (i_0,i_1) , where $i_0 \leq i \leq i_1$, indicating the subtrees rooted at the children of N from the i_0 -th to the i_1 -th. Starting from the i-th sub-tree, we add nearby sub-trees and check if they satisfy the ω -balance criterion. This involves iterating under all conditions (i_1,i_0) , where $0 < i_0 < i$ and $0 < i_1 < t$, stopping the iteration when $T(N.\mathbf{C}_{nl}[j]\}_{j=i_0}^{j=i_1}$) is balanced. Each time a new sub-tree is added, we update $\zeta = \mathcal{S}(T(N.\mathbf{C}_{nl}[j]\}_{j=i_0}^{j=i_1})$) and $\psi = (i_0,i_1)$ if the following condition is satisfied:

$$S(T(N.\mathbf{C}nl[j]^{j=i_1}j=i_0)) > \zeta.$$
(14)

Therefore, the corresponding b indicates the sub-trees rooted at the children of N that require reconstruction.

B. Insertion with Dynamic Rebalancing

After discussing the rebuilding scheme, we delve into its implementation in the insertion process, as outlined in Algorithm 3. The algorithm involves a backtracking approach for insertion. In the process of each backtrack, we examine whether N violates the ω -balance criterion and necessitates rebuilding using the selective sub-tree rebuilding scheme (lines 4-5) to identify which part needs to be rebuilt. Once identified, instead of using the entire dataset to retrain the two-stage regression model (see Section IV-B), we only use the changed dataset to update the model. For newly inserted data points, we denote them as $S_x^1 = \sum_{i=1}^{n_1'} x_i$, and for points allocated to other sub-trees, we represent them as $S_x^2 = \sum_{i=1}^{n_2'} x_i$. Hence, S_x' for updating can be expressed as:

$$S_x' = S_x + S_x^1 - S_x^2. (15)$$

Similarity, we can define the S'_u , S'_{xu} and S'_{x^2} . Hence, updating the root model parameter α is expressed as follows:

$$\alpha = \frac{(n' + n_1' - n_2') \times S_{xu}' - S_x' \times S_u'}{(n' + n_1' - n_2') \times S_{x2}' - (S_x')^2},$$
(16)

and then the expressions for updating β is as follows:

$$\beta = \frac{S_u' - \alpha \times S_x'}{(n' + n_1' - n_2')}. (17)$$

Therefore, we update the root model and allocate data points to each sub-model for training, thereby updating the two-stage regression model and making predictions for the pivot set. For inserting data points, repeatedly invoking the same function requires additional operations, such as restoring the execution state from the call stack, thereby increasing time costs. To mitigate the frequent invocation of the insertion function, we

```
Algorithm 3: In_Place_Insertion (\mathbf{D}_1, N, d')
```

```
Input: \mathbf{D}_1 \in \mathbb{R}^{n_1 \times d}: the new coming data, N: the node, d'
             is the tree depth.
 1 Default values: N \leftarrow the root node, d' \leftarrow 0.
 2 if D_1 is null then
        return;
 4 if N breaks the w-balanced-criterion then
         Rebuild the sub-tree rooted at N;
 5
 6 if N.isleaf then
         N.add(\mathbf{D}_1);
         if The number of vectors in N exceeds c then
              Split N into new leaf nodes;
10 else
         d' \leftarrow d' \mod d;
11
        \mathbf{D}^* \leftarrow [][] \ ;
                                            // 2-dimension array
12
         for i \leftarrow 0 up to |N.O| do
13
              for j \leftarrow 0 up to n_1 do
14
                   if N.O[i][d'] < p_i[d'] < N.O[i][d'] then
15
                     \mathbf{D}^*[i].add(\mathbf{p_j});
16
         \textbf{for each} \ i \leftarrow 0 \ \textit{up to} \ |N.\mathbf{O}| \ \textbf{do}
17
              In_Place_Insertion(\mathbf{D}^*[i], N, d'+1);
```

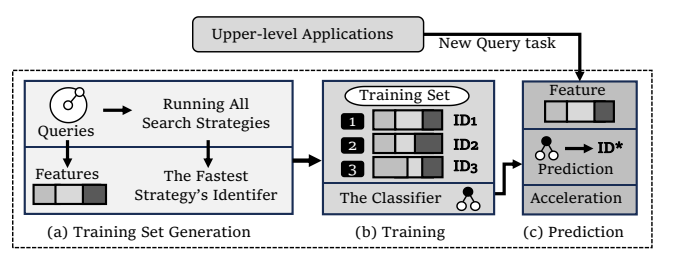


Fig. 6. Three modules in our auto-selection model.

bulk-load data points (lines 13-16). Specifically, we group the points belonging to a specific sub-space into a set and insert them into the corresponding sub-tree (line 18).

VI. SEARCH STRATEGY AUTO-SELECTION

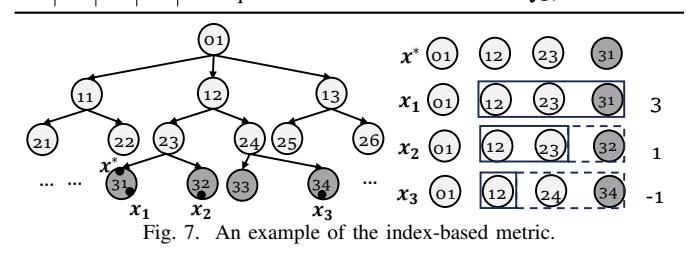
We design an auto-selection model to improve queries' efficiency by automatically selecting the optimal search strategy for the arbitrary query task. We initially present the search strategies for conducting $k{\rm NN}$ and radius searches over UnIS. Then, as shown in Fig. 6, we extract query meta-features from search tasks and generate class labels (i.e., ground truth) from the training logs, containing the best search strategy for each query. Next, we feed the query meta-features and class labels into a classification model to learn how to map from a query task to the best-performing strategy. Using the trained model, we predict the optimal strategy for new queries.

A. Search Strategies

Numerous factors could impact the query efficiency, and considering all possible factors in the search strategies is computationally impractical. Therefore, we narrow our focus to two key factors: traversal strategies (DFS or BFS) and the minimum bounding volume (MBB or MBR), resulting in four search strategies. Table II outlines the pruning strategies corresponding to each search strategy for kNN and radius search. For example, $R_{\rm DFS}$ represents a search strategy employing the DFS and the MBR. Specifically, in kNN search,

Algorithm 4: UnIS_kNN(\mathbf{q}, k, B, T)

```
Input: \mathbf{q}: the query point, k: an integer, B: the bounding
            volume, T: the traversal strategy.
   Output: Q: the bounded INqueue.
 1 Q \leftarrow empty priority queue of size k;
2 N \leftarrow root node;
3 if T is the DFS then
        \mathsf{DFS}(\mathbf{q}, N, B, k, Q);
5 else
        \mathsf{BFS}(\mathbf{q},\,N,\,B,\,k,\,Q);
7 return Q;
   Function DFS (\mathbf{q}, N, B, k, Q):
        if N is a leaf then
             foreach point p in N do
10
                  ED \leftarrow \operatorname{dist}(\mathbf{q}, \mathbf{p});
11
                  Q.add((\mathbf{p}, ED));
12
          ^{\prime}\star Lemma ^{1} is used.
        if pruning condition based on B is not met or
13
          Q.size() < k  then
             Recurse to child nodes;
14
Function BFS (q, N, B, k, Q):
        Q_1 \leftarrow queue initialized with N;
16
17
        while Q_1 is not empty do
             N \leftarrow Q_1.\mathsf{pop}();
18
             if N is a leaf then
19
20
                  foreach p in N do
21
                       ED \leftarrow \operatorname{dist}(\mathbf{q}, \mathbf{p});
                       Q.add((\mathbf{p}, ED));
22
             else
23
                  /\star~B= MBR uses Lemma 2, and B=
                       MBB uses Lemma 3.
                  if pruning condition based on B is not met or
24
                    Q.size() < k then
                       Enqueue all children of N into Q_1;
25
```



Lemma 3 is utilized to prune search spaces, while in radius search, Lemma 1 is employed for the same purpose. Due to space limitations, we only provide the kNN procedure here, while the detailed radius search process is included in the appendix (see Section IX-A). Specifically, in kNN, both traversal strategies and pruning are essential for query efficiency, whereas in radius search, only traversal strategies have a notable impact.

Algorithm 4 outlines the procedure for processing kNN queries. Depending on the traversal strategy, either DFS (line 4) or BFS (line 6) is used. In DFS, the algorithm recursively explores nodes starting from the root and processes all leaf nodes (lines 9–12). During traversal, pruning is performed using Lemma 1, regardless of whether B is MBR or MBB. If the pruning condition is not satisfied, the algorithm recurses to the child nodes (lines 13–14). In BFS, the algorithm processes nodes level by level, starting from the root and proceeding to its children. During the search, Lemma 2 is used when B is the MBR, and Lemma 3 is applied when B is the MBB.

Algorithm 5: Auto_Selection(\mathbf{D} , \mathcal{G})

```
Input: D: the dataset, G: the query task set.
   Output: z^*: the optimal search strategy.
 1 \mathcal{G}_0 \leftarrow Randomly generated query task set;
2 for each query task g \in \mathcal{G}_0 do
       Extracting features F from g;
 4
       for each search strategy z \in \mathbf{Z} do
           Running g using the search strategy z;
 5
       z^* \leftarrow the fast search strategy;
 6
       S.add(<F, z^*>);
8 Training the classifier on S;
  A new query task q;
10 \mathbf{F} \leftarrow extracting features from g;
11 Predicting the optimal search strategy z^* for q;
12 return z^*;
```

TABLE II PRUNING TECHNOLOGIES ON EACH SEARCH STRATEGY.

Pruning	$R_{ t DFS}$	$R_{ t BFS}$	$B_{ t DFS}$	$B_{ t BFS}$
kNN	Lemma 1	Lemma 2	Lemma 1	Lemma 3
Radius Search	Lemma 2	Lemma 1	Lemma 2	Lemma 1

B. Ground Truth Generation

- 1) Class Label Generation: We generate queries and process queries using different search strategies. For each query, we extract query meta-features and record the search strategy with the shortest execution time. Notably, we improve sample generation efficiency by terminating strategies that exceed the current best execution time u; otherwise, u is updated.
- 2) Query Meta-feature Extraction: Utilizing each value in the data point \mathbf{p}^* as a query meta-feature, denoted as \mathbf{F}_1 , is not informative enough. This limitation is evident in the auto-selection model utilized in the "AI+R"-tree [7], as depending solely on \mathbf{F}_1 does not result in high prediction accuracy. Hence, the sub-optimal strategy predicted by the model with low accuracy leads to an increase in query time.

Instead of only using \mathbf{F}_1 as the query meta-feature, we explore the relationships between each data point in the training sample \mathbf{X} to uncover the latent information \mathbf{F}_2 . Precisely, we learn graphical representations of \mathbf{X} by analyzing the similarity between points based on the index-based metric and building the undirected weighted graph. Derived from the positions of data points in the graph, we extract the graph-based feature of each query point, labeled as \mathbf{F}_2 . Then, we merge \mathbf{F}_1 and \mathbf{F}_2 into \mathbf{F} to describe a query task.

Graph Generation. We generate an undirected weighted graph $G = (\mathbf{X}, \mathbf{E})$ where each query point can be represented by a vertex $\mathbf{x}_i \in \mathbf{X}$. Vertices \mathbf{x}_i and \mathbf{x}_j are linked by an edge $e = (\mathbf{x}_i, \mathbf{x}_j) \in \mathbf{E}$, denoting the similarity between two instances, computed using the metric discussed below.

Index-based Metric. During insertion, each data point (or instance) is compared with the pivots and recursively assigned to sub-spaces. The more frequently points are allocated to the same sub-spaces, the more similar they are. Conversely, the more times they are distributed to different sub-spaces, the

more dissimilar they are. Hence, we propose the index-based metric to measure data point similarity:

Definition 11. (Index-based Metric) For each pair of instances \mathbf{x}_i and \mathbf{x}_j (where $i \neq j$), the index-based metric $\mathcal{I}(\mathbf{x}_i, \mathbf{x}_j)$ is calculated as the times they fall into the same sub-space minus the times they fall into different sub-spaces before reaching the leaf node. The expression is as follows:

$$\mathcal{I}(\mathbf{x}_i, \mathbf{x}_j) = \mathcal{T}^+(\mathcal{U}(\mathbf{x}_j), \mathcal{U}(\mathbf{x}_i)) - \mathcal{T}^-(\mathcal{U}(\mathbf{x}_j), \mathcal{U}(\mathbf{x}_i)) - 1, \quad (18)$$

where $\mathcal{U}(\mathbf{x}_i)$ denotes the node path from the root to the leaf node containing \mathbf{x}_i , $\mathcal{T}^+(\mathcal{U}(\mathbf{x}_i),\mathcal{U}(\mathbf{x}_j))$ represents the count of common nodes in the two paths, and $\mathcal{T}^-(\mathcal{U}(\mathbf{x}_i),\mathcal{U}(\mathbf{x}_j))$ signifies the count of different nodes in the two paths.

In Fig. 7, we apply t=3 to construct the index and label each sub-space in each partition. For example, during the first partition process, sub-spaces are labeled as "11", "12", and "13", representing the three sub-spaces (also known as subtrees). Then, we compute similarities between \mathbf{x}^* and each of \mathbf{x}_1 , \mathbf{x}_2 , and \mathbf{x}_3 . Each instance undergoes three partitions to reach a leaf node, and we count the times they fall into the same sub-space and different sub-spaces. For example, \mathbf{x}^* and \mathbf{x}_2 consistently fall into the same sub-space, such as "12" and "24", and into different sub-spaces, with \mathbf{x}^* traversing "31" and \mathbf{x}_2 traversing "32", resulting in $\mathcal{I} = (\mathbf{x}^*, \mathbf{x}_1) = 1$.

Feature Generation. Once the graph is constructed, the process of generating feature \mathbf{F}_2 unfolds as follows: Initially, an instance \mathbf{x} enters its corresponding leaf node. Then, edges between \mathbf{x} and other instances can be directly obtained based on the leaf node's position in the index. For example, in Fig. 7, if an instance resides in the "34" leaf node, the edge with all data points in the "31" leaf node is 1. Hence, to derive \mathbf{F}_2 , we traverse all leaf nodes and obtain a fixed-sized feature.

C. Model Training and Prediction

The process outlined in Algorithm 5 involves training the auto-selection model to predict the optimal search strategy, treating the strategy selection as a multi-class classification problem. Initially, we generate a set of query tasks \mathcal{G}_0 randomly (line 1). Each task undergoes query meta-feature extraction and execution using all available search strategies, with the fastest one identified as the optimal strategy z^* (lines 2–7). Next, using the ground truth, we train the multi-class classifier (line 8). Specifically, we use *ensemble learning* (EL) [52] (Random Forest [38] in the experiments), which combines the outputs of multiple learners to address the potential inaccuracies of individual classifiers. Once the auto-selection model is trained, it can predict the optimal search strategy for query processing (lines 9–11).

VII. EXPERIMENTS

A. Experimental Setup

Dataset. We evaluate our method on eight real-world datasets: ArgoPOI, ArgoAVL, Porto, Shapenet, T-drive, ArgoPC, Apollo, and ArgoTraj. All datasets were collected on edge devices; for example, ArgoPOI, ArgoAVL,

TABLE III
AN OVERVIEW OF DATASETS (M FOR MILLION).

Dataset	ArgoPOI	ArgoAV	L Porto	T-drive	Shapenet	ArgoPC	Apollo	ArgoTraj
Ref.	[3]	[3]	[6]	[51]	[5]	[3]	[2]	[3]
d	2	2	2	2	3	3	3	4
Scale	6M	2M	1.27M	1.27M	1M	10.00M	10.00M	2.70M

ArgoPC, and ArgoTraj were obtained from sensors mounted on vehicles, all from an autonomous driving dataset called Argoverse [3]. Table III summarizes the details.

Implementations. We implement Unis and all comparisons using Java 8 and evaluate performance on two platforms. The first platform is a server equipped with an i9-14900KF CPU and 128 GB RAM. In our experiments, 8 CPU cores are used. The server supports parameter learning and large-scale experiments, including indexing, insertion, and query performance. The second platform is a wheeled mobile robot, Wheeltec R550, which serves as an edge device to validate the superior performance of Unis. It is equipped with a Jetson Nano [1], which integrates a 64-bit ARM Cortex-A57@1.43 GHz and 4 GB of memory. The source code is available at [4] for reproducibility. Unless otherwise specified, we set $\delta = 0.01$ and l = 100 (see Section VII-B for details) for index construction, and our algorithm is single-threaded.

Comparisons. We first compare our method with existing indexing structures, including Ball-tree [31], BDL-tree [50], BMKD-tree [9], and "AI+R"-tree [7]. For search strategy auto-selection, we consider several SOTA models as competitors, including Unik [42], the auto-selection model in the "AI+R"-tree ("AI+R"-tree) [7], and TRIO [15]. All comparisons are discussed in Section II.

B. Index Construction

Parameter studies are conducted on the server due to its large computational capacity. We also use the Wheeltec R550 as an edge device to demonstrate the construction efficiency of Unis compared with SOTAs. Note that we evaluate the performance of the two-stage linear model; the detailed results are provided in the appendix (see Section IX-C).

Parameters Study. Table IV shows how the performance of our index varies under different parameter settings. Here, we only report the results on the ArgoPOI dataset, while the results for other datasets and the corresponding analysis are provided in the appendix (see Section IX-D). The baseline is set with $\delta = 1 \times 10^{-4}$ and l = 5. Specifically, t^1 denotes the construction time, t_{kNN}^1 denotes the runtime of kNN, and t_{RS}^1 denotes the runtime of radius search. For UnIS with different parameters, the construction time, kNN runtime, and radius search runtime are denoted as t^0 , t^0_{kNN} , and t^0_{RS} , respectively. Observations. We chose $\delta = 0.01$ because it offers a good balance between index construction and query efficiency, though not necessarily the optimal point for both. As the sample size increases, construction time first decreases due to more accurate pivot prediction and better-balanced trees, but later increases because of the higher overhead of processing larger samples. Query performance shows a similar trend: efficiency

TABLE IV
IMPACT OF PARAMETERS ON UNIS CONSTRUCTION.

Dataset	Parameters		Sampling Rate δ									# Models l								
		5×10^{-4}	1×10^{-3}	5×10^{-3}	1×10^{-2}	5×10^{-2}	1×10^{-1}	5×10^{-1}	10	50	100	500	1000	5000	10000					
ArgoPOI	$t_{k\mathrm{NN}}^0/t_{k\mathrm{NN}}^1$	0.55 1.00	0.39 0.83	0.32 0.17	0.24 0.17	0.26 0.00	0.29 0.00	0.80 0.50		0.86 1.52		0.83	0.78 1.30	0.77 1.55	0.84					
111 901 01	$t_{\mathrm{RN}}^{0}/t_{\mathrm{RS}}^{0}$	45.25	0.83	24.25	7.50	3.75	0.00	16.00	2.72				1.99	2.23	1.97					

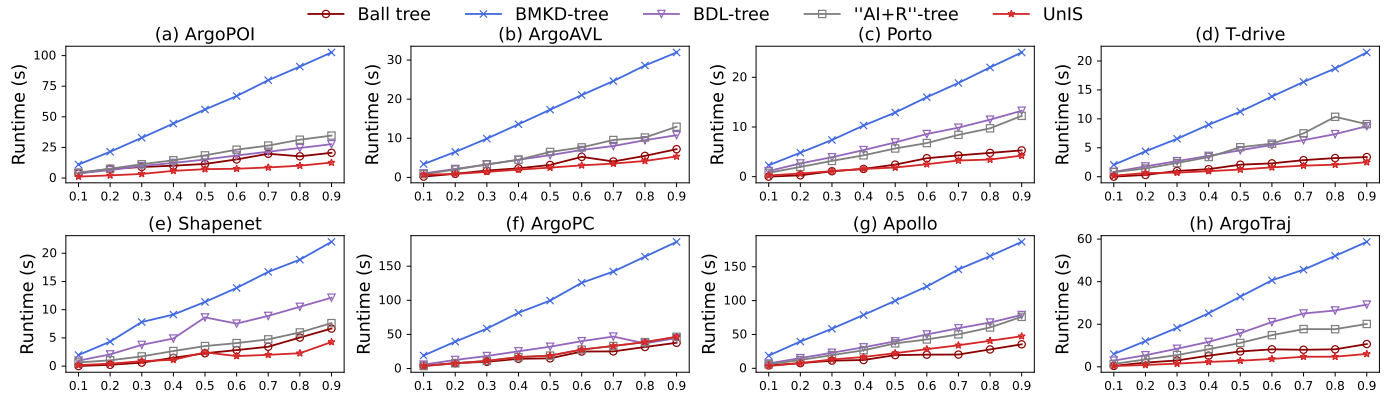


Fig. 8. Comparison of indexing time across different indexes.

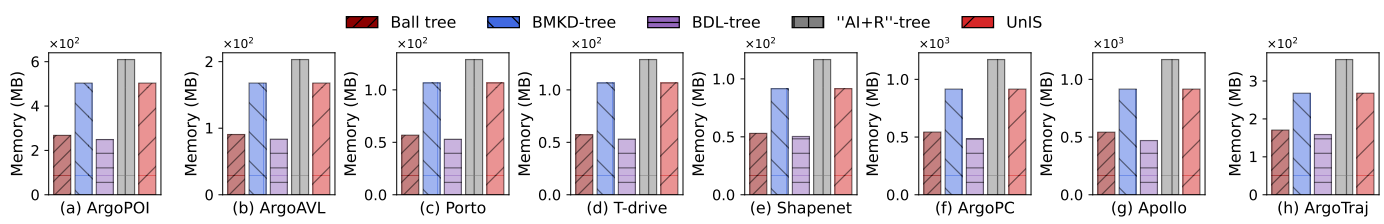


Fig. 9. The memory cost of each algorithm.

TABLE V The impact of two factors on $k{\rm NN}$ search

Dataset	ArgoPOI	ArgoAVI	Porto	Shapenet	T-drive	ArgoPC	Apollo	ArgoTraj
$\frac{t_{\mathrm{BFS}}}{t_{\mathrm{DFS}}}$	0.01	1.12	0.01	0.01	9.64	0.01	6.44	0.04
$\frac{t_{ m MBR}}{t_{ m MBB}}$	4.34	0.22	3.04	0.04	0.06	0.15	2.40	0.03

improves with more samples until the tree is sufficiently balanced, after which further increases bring little benefit. Moreover, we selected 100 sub-models as they offer a reasonable trade-off between index construction efficiency and query performance, even though this may not represent the optimal setting for both. As the number of sub-models increases, construction time first decreases due to more accurate pivot prediction and thus a more balanced tree, but then increases once the index is sufficiently balanced, since additional models add computational overhead without further improvement. Query efficiency follows the same trend: it improves as the index becomes more balanced, but eventually stabilizes.

Time Cost of Indexing. We study how the construction time changes with the increasing number of data points. We denote δ as the sampling rate, where $\delta \in (0,1)$. For example, with $\delta = 0.2$ and a dataset of 100 million data points, it means 20 million data points are used for index construction.

<u>Observations</u>. In Fig. 8, for most cases, the index construction time generally follows the order: Ball-tree > BMKD-tree > BDL-tree > "AI+R"-tree > UnIS.

However, on a few specific datasets, Unis does not achieve the shortest index construction time. This is primarily because, on smaller datasets, the cost of constructing the two-stage model constitutes a larger proportion of the total indexing time.

Memory Cost. We present a comparison of the memory usage of selected indexes over five datasets. In particular, "memory usage" represents the amount of memory occupied by Java during the index construction process.

<u>Observations</u>. In Fig. 9, the number of data points affects memory usage; larger datasets consume more memory. Compared with the BMKD-tree, our method requires slightly more memory because of the additional cost of constructing the two-stage linear regression model. However, this overhead is negligible relative to the dataset size.

C. Index Insertion

We first conduct a parameter study to examine the impact of δ and l on insertion performance, and then verify that UnIS achieves lower insertion latency than SOTAs.

Parameter Study. Table VI presents the insertion latency of our index under varying parameters.

<u>Observations</u>. Increasing δ initially reduces insertion latency and then causes it to rise. Small samples yield inaccurate pivot predictions and unbalanced sub-trees, while larger samples reduce tree depth, lowering reconstruction cost. Beyond a

TABLE VI IMPACT OF PARAMETERS ON INSERTION.

Dataset			S	ampling Rate	δ			# Models l							
Zuusee	5×10^{-4}	1×10^{-3}	5×10^{-3}	1×10^{-2}	5×10^{-2}	1×10^{-1}	5×10^{-1}	10	50	100	500	1000	5000	10000	
ArgoPOI	1.37	1.83	1.85	1.86	1.86	1.92	2.46	1.04	1.04	1.02	1.11	0.98	0.93	0.98	
ArgoAVL	1.22	1.22	1.30	1.24	1.29	1.39	1.78	1.03	1.02	1.06	1.06	1.01	0.95	0.99	
Porto	1.06	1.18	1.20	1.31	1.15	1.33	1.44	1.03	0.99	1.04	0.98	1.11	1.00	1.01	
T-drive	1.01	1.14	1.16	1.22	1.14	1.19	1.49	0.95	0.96	0.99	0.93	1.01	0.96	0.96	
Shapenet	1.01	1.07	1.02	1.06	0.99	1.05	1.34	1.02	0.99	1.00	1.11	0.95	1.00	1.10	
ArgoPC	1.02	1.02	1.02	1.06	1.05	1.10	1.44	1.02	0.97	0.98	0.96	0.98	1.06	0.98	
Apollo	1.07	1.11	1.23	1.18	1.20	1.29	1.66	0.93	0.96	0.94	0.96	1.05	0.93	0.91	
ArgoTraj	1.38	1.31	1.33	1.36	1.46	1.43	1.79	0.92	0.95	0.96	1.01	0.93	0.95	1.16	

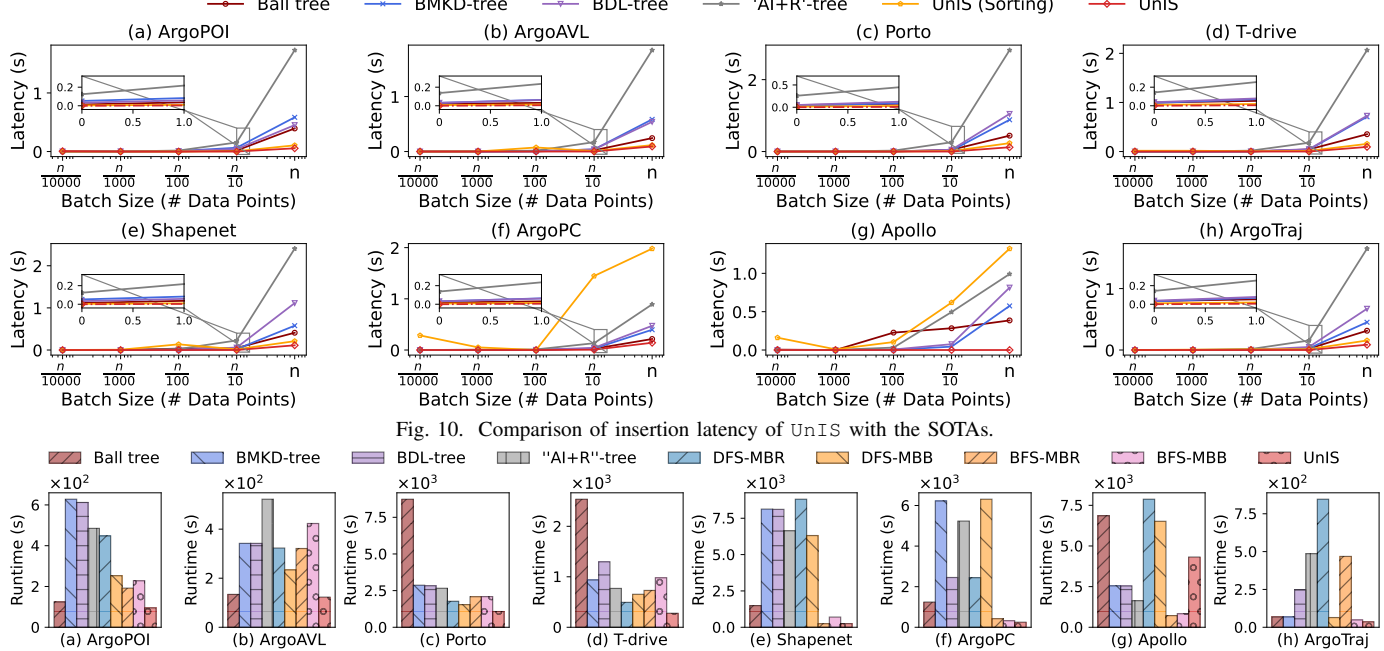


Fig. 11. Comparing the query runtime of UnIS with the SOTAs.

certain point, further increases provide little improvement in balance, and the overhead of handling more samples dominates, increasing latency. Similarly, as the number of submodels grows, sub-tree rebuilding latency first decreases due to more accurate pivot predictions and better balance, then rises as additional models add overhead without further benefit.

Insertion Latency. Our focus is on the latency of inserting a fixed number of data points. We investigate the variation in latency as the volume of inserted data points increases.

Observations. In Fig. 10, when the number of data points to

<u>Observations</u>. In Fig. 10, when the number of data points to be inserted is less than $\frac{n}{100}$, there is a minimal disparity in insertion efficiency between UnIS and the baselines. However, as the number of data points increases, the insertion efficiency of UnIS outperforms SOTAs.

D. Evaluation of Auto-selection Model

We first evaluate the auto-selection model and then verify it can accelerate queries. Due to space limitations, we verify its effectiveness in accelerating k-means in the appendix (see Section IX-E).

Impact of Key Factors. We focus on two factors, traversal methods and bounding volumes, to examine their impact

on query performance, as shown in Table V. Due to space limitations, we use $k{\rm NN}$ as a representative query. Notably, $\frac{t_{\rm BFS}}{t_{\rm DFS}}$ represents the ratio of the $k{\rm NN}$ query time using the BFS strategy to that using the DFS strategy, while $\frac{t_{\rm MBR}}{t_{\rm MBB}}$ represents the ratio of the $k{\rm NN}$ query time using the MBR strategy to that using the MBB strategy.

<u>Observations</u>. We found that across different datasets, traversal methods have a greater impact than minimum bounding volumes in kNN. This may be because, when the dataset is large and dense, adjacent nodes overlap heavily or lie very close to each other, making it difficult to prune branches or data points. In contrast, traversal methods determine the order in which data points are explored. If traversal begins near the query point, pruning becomes more effective because a tighter bound can be established earlier.

Ground Truth Generation. We divide 1×10^5 query samples into three parts: 80% for training, 10% for validation, and 10% for testing. Precisely, given a dataset **D** compressed by the MBR, denoted as $R = (\mathbf{lb}, \mathbf{ub})$, for kNN search, each query involves a query point \mathbf{x}^* and an integer k. We randomly select a data point \mathbf{x}^* from **D**, and k is chosen randomly from

TABLE VII PERFORMANCE OF THE PROPOSED FEATURE EXTRACTION METHOD.

Accuracy _		Unik		"AI	+R"-tr	ee	I	TRIO			UnIS		×Speedup
ricearacy -	\mathbf{F}_1	F F	-F ₁	\mathbf{F}_1	F	\mathbf{F} - \mathbf{F}_1	\mathbf{F}_1	F	\mathbf{F} - \mathbf{F}_1	\mathbf{F}_1	F	\mathbf{F} - \mathbf{F}_1	Лорессир
MRR	94.87	95.27	0.40	87.52	88.51	0.99	85.82 8	37.43	1.61	92.35	93.66	1.31	1.08
Ball tro	# Data Points # 0.0		# Data Points	109	# Data Points	×10 ⁸	0.00 mg 0.10 mg 1.00 m	# tring of the tri	×10 ⁹ S 1.00 S 0.10 S 0.01	FFS-MBR Data Doints 0.1	0	# Data Points	Unis ×10 ⁸
(a) ArgoF	OI	(b) ArgoAVL		(c) Porto	,	(d) T-drive	(e) Shap		(f) ArgoP((g) Apollo		(h) ArgoTraj

Fig. 12. The performance of kNN search of different indexes and search strategy in terms of # data points access.

TABLE VIII RADIUS SEARCH PERFORMANCE.

Dataset	Strategy	Percent	Prediction	Speedup
ArgoPOI	MBR-DFS	97.78%	0.01%	28.96%
ArgoAVL	MBR-DFS	96.74%	10.57%	37.09%
Porto	MBR-BFS	99.54%	0.02%	30.92%
Shapenet	MBR-BFS	97.77%	0.02%	33.99%
T-drive	MBR-BFS	97.74%	0.01%	30.53%
ArgoPC	MBR-DFS	98.04%	18.98%	36.76%
Apollo	MBR-DFS	97.87%	28.96%	25.59%
ArgoTraj	MBR-DFS	98.67%	12.17%	36.06%

the range 1 to 1000. Similarly, for radius search, each query comprises a point \mathbf{p}^* and a radius r. We randomly select a point \mathbf{p}^* from \mathbf{D} , and compute r as $r = \sum_{i=1}^d (ub_i - lb_i)^2 \times \tau$, where τ is randomly selected from the interval [0, 1].

Verification for Feature Extraction. We use the mean reciprocal rank (MRR) [42] to assess the auto-selection model performance. The empirical results are presented in Table VII. *Observations*. (1) The addition of features extracted by our feature extraction method results in improved predictive accuracy in most cases, as evaluated by different metrics. However, not all additional features improve prediction accuracy, as the extracted features may not always contain useful information. (2) In most cases, using our auto-selection model to predict the effective search strategy yields the highest prediction accuracy.

kNN and Radius Search Performance. The runtime of a query consists of the query execution time and the prediction time. Additional costs from index construction and periodic insertions are excluded, as construction is performed offline. Including insertion costs would introduce variability across different indexes, which could distort an accurate comparison of the intrinsic query performance of each method. For kNN search, the evaluation metrics are the runtime and the number of data point accesses, both reported as averages per query. For radius search, certain strategies dominate as the fastest in several datasets, causing the prediction model to consistently favor a single strategy. However, it still serves as an effective means to eliminate inefficient strategies. In Table VIII, we report the most frequently selected strategy across a set of radius search tasks (denoted as "Strategy"), its selection ratio

(denoted as "Percent"), and the proportion of prediction time in the total query time (denoted as "Prediction"). Moreover, we also report the corresponding time improvement relative to the average runtime of all search strategies. Notably, the runtime of a single query consists of two recurring components: query execution time and prediction time. The following experiments do not consider index construction, which can be performed offline, nor insertion performance, since insertion latency would hinder the evaluation of UnIS 's query efficiency. Observations. (1) Fig. 11 shows our auto-selection model improves kNN efficiency. However, it does not achieve the best performance all the time. For instance, in ArgoPC, the model is slower than using BFS-MBB. This is because the minor performance gains are offset by the additional time required for prediction. (2) Fig. 12 shows that the search strategies chosen by the auto-selection model traverse the fewest points. However, this differs from Fig. 11 because fewer traversed points do not mean shorter running time, as the total time includes both query and prediction times. (3) In Table VIII, when the most frequently selected strategy dominates with a significantly higher proportion, UnIS still improves search efficiency compared to the average runtime of all strategies.

VIII. CONCLUSIONS AND FUTURE WORK

In this paper, we presented UnIS for efficient on-device search. We first designed a partition method and a lightweight ML model to improve the BMKD-tree construction efficiency. We then proposed a real-time in-place insertion operation to enable queries to access continuously generated data points. Furthermore, we proposed an auto-selection model to improve search efficiency. Experiments showed that UnIS effectively improved the efficiency of indexing, insertion, and on-device search. In future work, we plan to extend UnIS to a parallel framework to better use computational resources. We also investigate which dataset distributions benefit most from the auto-selection model in accelerating on-device search.

ACKNOWLEDGMENTS

This work was supported by the National Key R&D Program of China (2023YFB4503600), National Natural Science Foundation of China (62202338, 62372337), and the Key R&D Program of Hubei Province (2023BAB081).

REFERENCES

- [1] Nvidia jetson nano. https://developer.nvidia.com/embedded/jetson-nano.
- [2] Public datasets for autonomous driving. https://apolloscape.auto/.
- [3] Public datasets for perception and prediction in driving scenes. https://www.argoverse.org/index.html.
- [4] Repository of UnIS. https://github.com/whu-totemdb/UnIS.
- [5] Shapenet. https://shapenet.org/.
- [6] Taxi service trajectory prediction challenge 2015. https://figshare.com/ articles/dataset/Porto_taxi_trajectories/12302165.
- [7] A. Al-Mamun, C. M. R. Haider, J. Wang, and W. G. Aref. The "AI + R"-tree: An instance-optimized R-tree. In MDM, pages 9–18, 2022.
- [8] J. L. Bentley. Multidimensional binary search trees used for associative searching. *Commun. ACM*, 18(9):509–517, 1975.
- [9] N. Bereczky, A. Duch, K. Németh, and S. Roura. Quad-kd trees: A general framework for kd trees and quad trees. *Theor. Comput. Sci.*, 616:126–140, 2016.
- [10] G. E. Blelloch and M. Dobson. Parallel nearest neighbors in low dimensions with batch updates. In ALENEX, pages 195–208, 2022.
- [11] Q. Cai, C. Cui, Y. Xiong, W. Wang, Z. Xie, and M. Zhang. A survey on deep reinforcement learning for data processing and analytics. *IEEE Trans. Knowl. Data Eng.*, 35(5):4446–4465, 2023.
- [12] Y. Cai, W. Xu, and F. Zhang. ikd-tree: An incremental K-D tree for robotic applications. arXiv preprint arXiv:2102.10808, 2021.
- [13] M.-F. Chang, J. Lambert, P. Sangkloy, J. Singh, S. Bak, A. Hartnett, D. Wang, P. Carr, S. Lucey, D. Ramanan, and J. Hays. Argoverse: 3D Tracking and Forecasting with Rich Maps. In CVPR, pages 8748–8757, 2019.
- [14] Y. Chen, B. Ivanovic, and M. Pavone. Scept: Scene-consistent, policy-based trajectory predictions for planning. In CVPR, pages 17082–17091, 2022
- [15] N. Cohen-Shapira and L. Rokach. Trio: Task-agnostic dataset representation optimized for automatic algorithm selection. In *ICDM*, pages 81–90, 2021.
- [16] J. H. Friedman, J. L. Bentley, and R. A. Finkel. An algorithm for finding best matches in logarithmic expected time. ACM Trans. Math. Softw., 3(3):209–226, 1977.
- [17] I. Galperin and R. L. Rivest. Scapegoat trees. In SODA, pages 165–174, 1993.
- [18] T. Gu, K. Feng, G. Cong, C. Long, Z. Wang, and S. Wang. The rlr-tree: A reinforcement learning based r-tree for spatial data. *Proc. ACM Manag. Data*, 1(1):63:1–63:26, 2023.
- [19] W. He, Z. Jiang, M. Kriby, Y. Xie, X. Jia, D. Yan, and Y. Zhou. Quantifying and reducing registration uncertainty of spatial vector labels on earth imagery. In KDD, pages 554–564, 2022.
- [20] Q. Hu, B. Yang, L. Xie, S. Rosa, Y. Guo, Z. Wang, N. Trigoni, and A. Markham. RandLA-Net: Efficient Semantic Segmentation of Large-Scale Point Clouds. In CVPR, pages 11105–11114, 2020.
- [21] Y. Ji, Z. Liu, S. Wang, Y. Sun, and Z. Peng. On simplifying large-scale spatial vectors: Fast, memory-efficient, and cost-predictable k-means. In *ICDE*, pages 863–876, 2025.
- [22] Y. Ji, S. Zhu, S. Huang, Z. Liu, S. Wang, and Z. Peng. Federated and balanced clustering for high-dimensional data. *Proc. VLDB Endow.*, 18(11):4032–4044, 2025.
- [23] T. Kraska, A. Beutel, E. H. Chi, J. Dean, and N. Polyzotis. The case for learned index structures. In SIGMOD, pages 489–504, 2018.
- [24] H. Lan, Z. Bao, J. S. Culpepper, and R. Borovica-Gajic. Updatable learned indexes meet disk-resident DBMS - from evaluations to design choices. *Proc. ACM Manag. Data*, 1(2):139:1–139:22, 2023.
- [25] I. Lang, A. Manor, and S. Avidan. SampleNet: Differentiable point cloud sampling. In CVPR, pages 7578–7588, 2020.
- [26] J. Li, H. Liu, C. Gui, J. Chen, Z. Ni, and N. Wang. The design and implementation of a real time visual search system on JD e-commerce platform. arXiv preprint arXiv:1908.07389, 2019.
- [27] R. Li, S. Wang, F. Zhu, and J. Huang. Adaptive graph convolutional neural networks. In AAAI, pages 3546–3553, 2018.
- [28] S. P. Lloyd. Least squares quantization in PCM. IEEE Transactions on Information Theory, 28(2):129–137, 1982.
- [29] L. H. Matthies, A. Huertas, Y. Cheng, and A. E. Johnson. Stereo vision and shadow analysis for landing hazard detection. In *ICRA*, pages 2735– 2742, 2008.
- [30] R. Neininger, K. Leckey, and W. Szpankowski. Towards more realistic probabilistic models for data structures: The external path length in tries under the markov model. In SODA, pages 877–886, 2013.

- [31] S. M. Omohundro. Five balltree construction algorithms. International Computer Science Institute Berkeley, 1989.
- [32] J. J. Pan, J. Wang, and G. Li. Survey of vector database management systems. VLDB J., 33(5):1591–1615, 2024.
- [33] O. Procopiuc, P. K. Agarwal, L. Arge, and J. S. Vitter. Bkd-tree: A dznamic scalable kd-tree. In SSTD, volume 2750, pages 46–65, 2003.
- [34] C. R. Qi, H. Su, K. Mo, and L. J. Guibas. PointNet: Deep Learning on Point Sets for 3D Classification and Segmentation. In CVPR, pages 652–660, 2017.
- [35] A. Sarfi, Z. Karimpour, M. Chaudhary, N. M. Khalid, M. Ravanelli, S. Mudur, and E. Belilovsky. Simulated annealing in early layers leads to better generalization. In CVPR, pages 20205–20214, 2023.
- [36] Q. Song, G. Wang, and C. Wang. Automatic recommendation of classification algorithms based on data set characteristics. *Pattern Recognit.*, 45(7):2672–2689, 2012.
- [37] R. Stern, T. Kulberis, A. Felner, and R. Holte. Using lookaheads with optimal best-first search. In AAAI, pages 185–190, 2010.
- [38] J. Su and H. Zhang. A fast decision tree learning algorithm. In AAAI, pages 500–505, 2006.
- [39] J. Van Brummelen, M. O'Brien, D. Gruyer, and H. Najjaran. Autonomous vehicle perception: The technology of today and tomorrow. Transportation research part C: emerging technologies, 89:384–406, 2018.
- [40] J. Wang, X. Yi, R. Guo, H. Jin, P. Xu, S. Li, X. Wang, X. Guo, C. Li, X. Xu, K. Yu, Y. Yuan, Y. Zou, J. Long, Y. Cai, Z. Li, Z. Zhang, Y. Mo, J. Gu, R. Jiang, Y. Wei, and C. Xie. Milvus: A purpose-built vector data management system. In SIGMOD, pages 2614–2627, 2021.
- [41] S. Wang, Z. Bao, J. S. Culpepper, and G. Cong. A survey on trajectory data management, analytics, and learning. ACM Comput. Surv., 54(2):39:1–39:36, 2022.
- [42] S. Wang, Y. Sun, and Z. Bao. On the efficiency of k-means clustering: Evaluation, optimization, and algorithm selection. *Proc. VLDB Endow.*, 14(2):163–175, 2020.
- [43] Y. Wang, H. Ma, and D. Z. Wang. LIDER: an efficient high-dimensional learned index for large-scale dense passage retrieval. *Proc. VLDB Endow.*, 16(2):154–166, 2022.
- [44] C. Wei, B. Wu, S. Wang, R. Lou, C. Zhan, F. Li, and Y. Cai. Analytical-v: A hybrid analytical engine towards query fusion for structured and unstructured data. *Proc. VLDB Endow.*, 13(12):3152–3165, 2020.
- [45] D. H. Wolpert and W. G. Macready. No free lunch theorems for optimization. *IEEE Trans. Evol. Comput.*, 1(1):67–82, 1997.
- [46] A. Xiao, X. Zhang, L. Shao, and S. Lu. A survey of label-efficient deep learning for 3d point clouds. *IEEE Trans. Pattern Anal. Mach. Intell.*, 46(12):9139–9160, 2024.
- [47] J. Xu, Z. Bao, and H. Lu. A framework to support continuous range queries over multi-attribute trajectories. *IEEE Trans. Knowl. Data Eng.*, 35(2):1119–1133, 2023.
- [48] T. Xu, B. Tian, and Y. Zhu. Tigris: Architecture and algorithms for 3d perception in point clouds. In MICRO, pages 629–642, 2019.
- [49] Y. Xu, H. Liang, J. Li, S. Xu, Q. Chen, Q. Zhang, C. Li, Z. Yang, F. Yang, Y. Yang, P. Cheng, and M. Yang. Spfresh: Incremental in-place update for billion-scale vector search. In SOSP, pages 545–561, 2023.
- [50] R. Yesantharao, Y. Wang, L. Dhulipala, and J. Shun. Parallel batch-dynamic kd-trees. arXiv preprint arXiv:2112.06188, 2021.
- [51] J. Yuan, Y. Zheng, C. Zhang, W. Xie, X. Xie, G. Sun, and Y. Huang. T-drive: Driving directions based on taxi trajectories. In GIS, pages 99–108, 2010.
- [52] C. Zhao, D. Wu, J. Huang, Y. Yuan, H. Zhang, R. Peng, and Z. Shi. Boosttree and boostforest for ensemble learning. *IEEE Trans. Pattern Anal. Mach. Intell.*, 45(7):8110–8126, 2023.
- [53] Y. Zhao, M. Li, L. Lai, N. Suda, D. Civin, and V. Chandra. Building a balanced k-d tree in o(kn log n) time. arXiv preprint arXiv:1410.5420, 2014.
- [54] Y. Zhu, L. Chen, Y. Gao, and C. S. Jensen. Pivot selection algorithms in metric spaces: a survey and experimental study. VLDB J., 31(1):23–47, 2022.
- [55] Y. Zhu, L. Chen, Y. Gao, B. Zheng, and P. Wang. DESIRE: an efficient dynamic cluster-based forest indexing for similarity search in multimetric spaces. *Proc. VLDB Endow.*, 15(10):2121–2133, 2022.

IX. APPENDIX

A. Radius Search

Algorithm 6 describes the radius search procedure using DFS (line 3) or BFS (line 5). In DFS, the algorithm recursively explores nodes, pruning subtrees using Lemma 2 (line 9). At the leaves (line 10), candidate points are checked, and those within the radius are added to the result set (line 13). Traversal continues recursively with child nodes (lines 16–18). In BFS, nodes are processed level by level: the root node is enqueued (line 21), nodes are expanded iteratively (lines 22–23), subtrees are pruned when possible using Lemma 1 (line 25), leaf points are tested and added to the result set (lines 26–29), and non-leaf children are enqueued for further exploration (lines 32–34).

```
Algorithm 6: Radius_Search(Q, T)
   Input: Q: query ball, T: traversal strategy.
   Output: P: result set.
 1 P \leftarrow \emptyset, N \leftarrow \text{the root node};
{f 2} if T is depth-first search then
        \mathsf{DFS}(Q, N, P);
 3
4 else
        BFS(Q, N, P);
 6 return P;
   Function DFS (Q, N, P):
        if N is pruned by is pruned by Lemma 2 then
            return:
10
        if N is leaf then
            foreach p \in N do
11
                 if p \in Q then
12
                      P \leftarrow P \cup \{p\};
13
            return:
14
        if N.left \neq \emptyset then
15
            \mathsf{DFS}(Q, N.left, P);
16
        if N.right \neq \emptyset then
17
             \mathsf{DFS}(Q, N.right, P);
18
19 Function BFS (Q, N, P):
        Q \leftarrow \text{empty queue};
20
        Q.add(N);
21
        while Q is not empty do
22
23
             U \leftarrow Q.poll();
             if U is pruned by Lemma 1 then
24
                 continue:
25
             if U is leaf then
26
                 foreach p \in U do
27
                      if p \in Q then
28
                         P \leftarrow P \cup \{p\};
29
             else
30
                 if U.left \neq \emptyset then
31
                      Q.add(U.left);
32
                 if U.right \neq \emptyset then
33
                      Q.add(U.right);
34
```

B. Wheeltec R550

The R550 (shown in Fig. 13) is a wheeled mobile robot with multiple chassis options, equipped with cost-effective sensors such as radar and depth cameras, making it suitable for learning applications in mapping and navigation, deep learning, 3D vision, and multi-robot coordination. Notably,



Fig. 13. Deployment of UnIS on Wheeltec R550.

it is powered by a Jetson Nano [1] as the main processor, featuring a 64-bit ARM Cortex-A57@1.43GHz and 4GB of memory.

C. Evaluating Two-Stage Regression Model

There is a trade-off between quantile prediction accuracy and runtime. However, a slight reduction in accuracy can lead to substantial improvements in efficiency. Specifically, we define the prediction error as $r=|{\rm actual}|$ quantile – predicted quantile|. A larger r indicates lower accuracy, while a smaller r corresponds to higher accuracy. For each dataset, we extract each dimension as an array and predict the median of each array to evaluate the accuracy of our method. Details are discussed below.

<u>Observations</u>. As shown in Table IX, our two-stage linear model achieves a prediction error r of less than 1%. In some cases, the model can directly predict the exact position of the median; for example, in the first dimension of the ArgoPOI dataset treated as an array, the prediction error is 0.

D. Parameter Study

The goal of our experiments was not to identify a universally applicable parameter setting, but rather to examine how the performance of our index changes with parameter variation. As shown in Table X, the baseline is defined with $\delta=1\times 10^{-4}$ and l=5. Specifically, t^1 denotes the construction time, $t^1_{k\rm NN}$ the runtime of $k\rm NN$ search, and $t^1_{\rm RS}$ the runtime of radius search. For UnIS built with different parameters, the corresponding times are denoted as t^0 , $t^0_{k\rm NN}$, and $t^0_{\rm RS}$, respectively. A detailed discussion is provided below.

TABLE IX
THE ACCURACY OF OUR TWO-STAGE LINEAR MODEL.

Accuracy	Accuracy ArgoPOI A		Argo	ArgoAVL Porto		orto	T-drive		Sha	Shapenet		Aı	ArgoPC		Apollo			ArgoTraj			
•	1th	2th	1th	2th	1th	2th	1th	2th	1th	2th	3th	4th									
\overline{r}	0	2.01E-10	3.58E-07	1.01E-06	1.22E-1	10 5.78E-10	1.53E-09	2.75E-10	4.70E-10	6.30E-10	0 (5.04E-08	3.10E-09	0	1.06E-07	3.21E-08	8 0	4.71E-08	3.73E-07	3.60E-07	4.64E-07

TABLE X IMPACT OF PARAMETERS ON UNIS.

	Parameters		Sampling Rate δ									# Models l							
		5×10^{-4}	1×10^{-3}	5×10^{-3}	1×10^{-2}	5×10^{-2}	1×10^{-1}	5×10^{-1}	10	50	100	500	1000	5000	10000				
	$\frac{t^0}{t^1}$	0.70	0.70	0.61	0.57	0.55	1.61	1.75	0.49	0.48	0.47	0.48	0.45	0.46	0.45				
ArgoPOI	$t_{k\mathrm{NN}}^0/t_{k\mathrm{NN}}^1$	1.00	0.83	0.77	0.77	0.77	0.77	0.77	0.87	0.87	0.87	0.87	0.87	0.87	0.87				
	$t_{ m RS}^0/t_{ m RS}^0$	0.75	0.75	0.73	0.73	0.73	0.73	0.73	2.72	2.49	0.99	0.99	0.99	0.99	0.99				
	$\frac{t^0}{t^1}$	0.79	0.68	0.79	0.81	0.68	1.65	1.77	0.53	0.55	0.63	0.56	0.40	0.35	0.38				
ArgoAVL	$t_{k\mathrm{NN}}^0/t_{k\mathrm{NN}}^1$	1.21	1.13	1.17	0.91	0.63	0.63	0.65	0.92	0.92	0.92	0.92	1.00	1.01	0.94				
	$t_{\rm RS}^0/t_{\rm RS}^0$	0.90	0.91	0.91	0.91	0.91	0.91	0.91	1.00	1.00	0.99	0.99	0.99	0.99	0.99				
	$\frac{t^0}{t^1}$	0.81	0.67	0.63	0.55	0.57	0.54	0.65	0.45	0.45	0.42	0.40	0.40	0.37	0.37				
Porto	$t_{k\mathrm{NN}}^0/t_{k\mathrm{NN}}^1$	0.89	0.84	0.83	0.89	0.87	0.89	0.87	1.00	1.00	1.00	1.00	1.00	1.00	1.00				
	$t_{\rm RS}^0/t_{\rm RS}^0$	0.96	1.17	0.99	0.97	0.97	0.97	0.97	0.89	0.89	0.89	0.89	0.89	0.70	0.74				
	$\frac{t^0}{t^1}$	0.97	0.74	0.67	0.61	0.58	0.64	0.92	0.58	0.53	0.53	0.54	0.48	0.63	0.66				
Shapenet	$t_{k\mathrm{NN}}^0/t_{k\mathrm{NN}}^1$	1.00	1.00	1.00	1.00	1.00	1.00	1.00	0.90	0.90	0.90	0.90	0.88	0.88	0.88				
	$t_{ m RS}^0/t_{ m RS}^1$	0.98	0.98	0.98	0.98	0.96	0.96	0.96	1.00	1.00	1.00	1.00	1.00	0.99	0.99				
	$\frac{t^0}{t^1}$	0.86	0.67	0.59	0.55	0.51	0.44	0.47	0.33	0.31	0.27	0.27	0.21	0.17	0.19				
T-drive	$t_{k\mathrm{NN}}^0/t_{k\mathrm{NN}}^1$	1.00	1.00	1.00	1.00	1.00	0.00	1.00	0.98	0.97	0.98	0.97	0.97	0.97	0.97				
	$t_{ m RS}^0/t_{ m RS}^1$	0.92	0.92	0.83	0.83	0.83	0.83	0.83	0.93	0.93	0.93	0.93	0.93	0.93	0.93				
	$\frac{t^0}{t^1}$	0.90	0.93	0.84	0.73	0.71	0.73	1.07	0.51	0.50	0.47	0.34	0.31	0.39	0.42				
ArgoPC	$t_{k\mathrm{NN}}^0/t_{k\mathrm{NN}}^1$	0.78	0.76	0.78	0.78	0.78	0.78	0.78	0.99	0.99	0.99	0.99	0.99	0.99	0.99				
	$t_{ m RS}^0/t_{ m RS}^1$	0.92	0.92	0.92	0.89	0.89	0.89	0.90	0.93	0.93	0.92	0.92	0.92	0.92	0.92				
	$\frac{t^0}{t^1}$	0.78	0.77	0.69	0.68	0.57	0.67	0.78	0.53	0.47	0.41	0.43	0.39	0.28	0.34				
Apollo	$t_{k\mathrm{NN}}^0/t_{k\mathrm{NN}}^1$	0.92	0.90	0.90	0.90	0.91	0.89	0.89	0.99	0.99	0.99	0.97	0.97	0.97	0.97				
	$t_{\rm RS}^0/t_{\rm RS}^1$	0.88	0.86	0.85	0.87	0.85	0.84	0.87	0.92	0.92	0.92	0.91	0.91	0.91	0.90				
	$\frac{t^0}{t^1}$	0.89	0.75	0.72	0.61	0.63	0.51	0.64	0.44	0.41	0.39	0.38	0.35	0.34	0.38				
ArgoTraj	$t_{k\mathrm{NN}}^{0}/t_{k\mathrm{NN}}^{1}$	0.87	0.87	0.87	0.87	0.87	0.87	0.87	0.90	0.82	0.82	0.86	0.86	0.82	0.85				
	$t_{ m RS}^0/t_{ m RS}^1$	1.00	1.00	1.00	1.00	1.00	1.00	1.00	1.00	1.00	1.00	1.00	1.00	1.00	1.00				

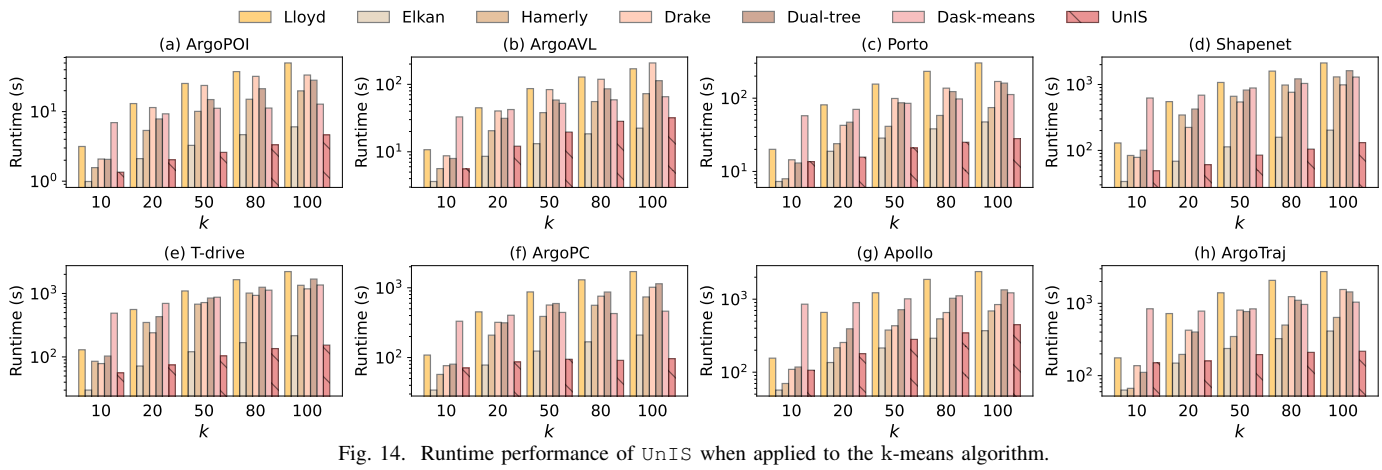
Observations. (1) First, as the number of sampled points increases, the index construction time initially decreases and then increases. When the sampling rate is small (e.g., 10^{-4}), pivot prediction is less accurate, yielding a less balanced index. With larger samples, prediction improves, producing a more balanced index with reduced depth and lower computation cost. However, when the sampling rate continues to increase, the index balance no longer improves significantly, while the computational overhead of handling larger samples increases, which in turn raises the overall construction time. (2) As the sampling rate increases, query efficiency generally improves. However, a larger sample size does not always guarantee higher search efficiency, since once the tree becomes sufficiently balanced. (3) As the number of sub-models increases, index construction time first decreases and then increases. With fewer sub-models (e.g., 10), pivots are predicted less accurately, producing a less balanced index. As the number grows, pivot prediction improves, the index becomes more balanced

with fewer levels, and construction cost decreases. However, once the index is sufficiently balanced, further increases add computational overhead without improving balance, which raises construction time. (4) As the number of sub-models increases, query efficiency generally improves. However, once the tree is balanced, adding more sub-models does not further reduce query time, which stabilizes within a certain range.

E. Verification for k-means

We demonstrate the effectiveness of UnIS when applied to k-means by comparing its runtime with other algorithms on edge devices. We follow the approach in [21], which proposes using two tree-based indexes to store data points and nodes, and leverages $k{\rm NN}$ to avoid unnecessary distance computations. Specifically, we evaluate performance using different values of $k \in \{10, 20, 50, 80, 100\}$

<u>Observations</u>. As shown in Fig. 14, when k is small (e.g., k=10), UnIS performs better than most SOTAs in pruning in most cases, but it's not always the best. For example, Elkan



outperforms it because UnIS requires additional time to construct our indexes, while kNN on these indexes is inefficient when k is small. Whereas when k is large, UnIS demonstrates superior runtime performance due to the effective pruning power of the centroid index.